

Electronic Supporting Information

Oxygen Binding Energy of Doped Metal: A Shortcut to Efficient Ni- Based Bimetallic Catalysts for Hydrodeoxygenation Reaction

Lifang Chen, Wei Liu, Haisong Feng, Yingyu Ren, Chunyuan Chen, Si Wang, Pan Yin, Yusen
Yang,* Xin Zhang,* Min Wei

*State Key Laboratory of Chemical Resource Engineering, Beijing Advanced Innovation Center for Soft
Matter Science and Engineering, Beijing University of Chemical Technology, Beijing 100029, P. R.
China*

* Corresponding authors. Tel: +86-10-64412131; Fax: +86-10-64425385.

E-mail addresses: yangyusen@mail.buct.edu.cn (Y. Yang); zhangxin@mail.buct.edu.cn (X. Zhang).

Table S1. Lattice parameters (in Å) of bulk Ni as calculated with PBE and DFT-D3 functionals and comparison to experiment

Method	Lattice constant
PBE	3.517
Expt ¹ .	3.524

Table S2. The optimized cell parameters of the bulk Ni-M (from Sc to Mo)

Doped Metal	a/Å	b=c/Å	Element	a=c/Å	b/Å
Sc	3.184↓	4.371↓	Y	3.443↓	4.588↑
Ti	3.474↓	3.849↑	Zr	3.145↓	4.529↑
V	3.708↑	3.511↓	Nb	3.787↑	3.808↑
Cr	3.722↑	3.394↓	Mo	3.843↑	3.646↑
Mn	3.581↑	3.462↓	Ru	3.650↑	3.648↑
Fe	3.563↑	3.497↓	Rh	3.704↑	3.562↑
Co	3.567↑	3.443↓	Pd	3.773↑	3.607↑
Cu	3.516↓	3.511↓	Ag	3.814↑	3.796↑
Zn	3.328↓	3.727↑			

Table S3. The mixing energies of bimetal models

Doped Metal	Mixing Energy/eV*	Doped Metal	Mixing Energy/eV
Sc	-1.98	Y	-1.21
Ti	-1.43	Zr	-1.43
V	-0.72	Nb	-1.08
Cr	-0.19	Mo	-0.37
Mn	--	Ru	0.76
Fe	-0.23	Rh	-0.13
Co	-0.03	Pd	-0.20
Cu	0.17	Ag	0.69
Zn	-1.04		

* $E_{mixing} = E_{total} - mE_{Ni_{bulk}} - nE_{M_{bulk}}$ m, n is the number of Ni atom and doped metal atom in bimetal bulk.

Table S4. The magnetic moment of Mn in NiMn and the corresponding to the energy, respectively

MAGMOM (Mn)	3	5	7	Spin polarization
Energy(eV) of NiMn(111)	-461.578	-461.581	-461.582	-461.667

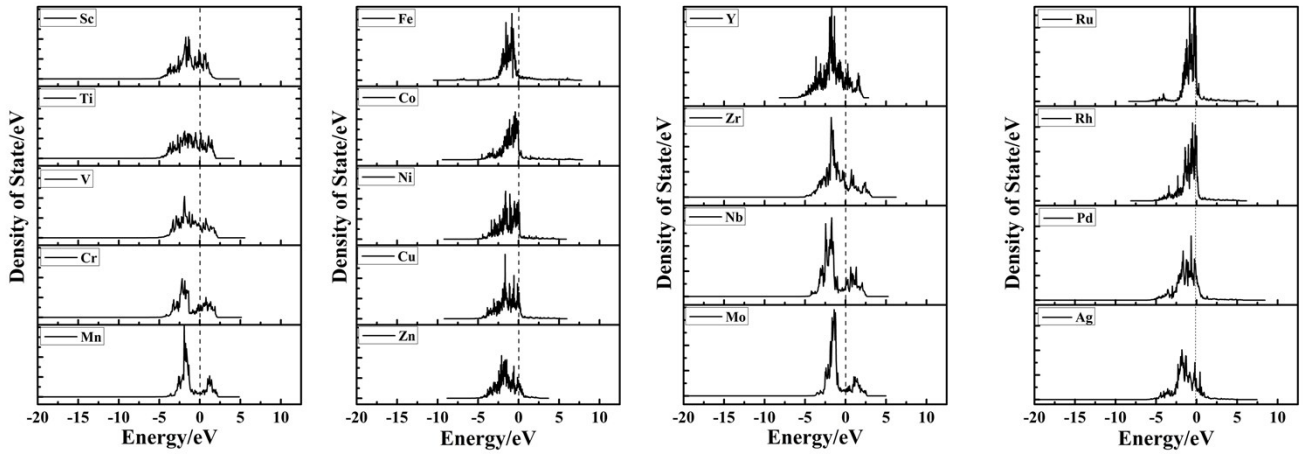


Figure S1. The projected density of state of Ni on Ni-M (111) surface. Dash line respects Fermi energy.

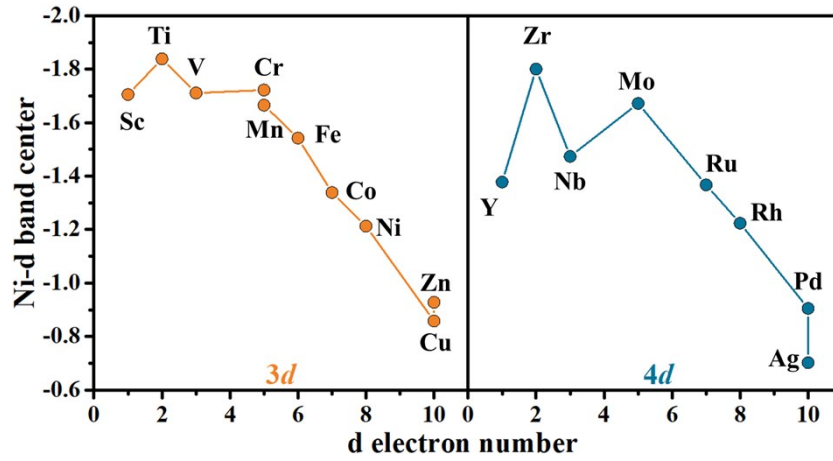


Figure S2. The d band center^a shift of parent metal Ni after addition of M in Ni-M (111).

^a The d band center² is calculated by

$$\varepsilon_d = \frac{\int_{-\infty}^{\infty} n_d(\varepsilon)\varepsilon d\varepsilon}{\int_{-\infty}^{\infty} n_d(\varepsilon)d\varepsilon}$$

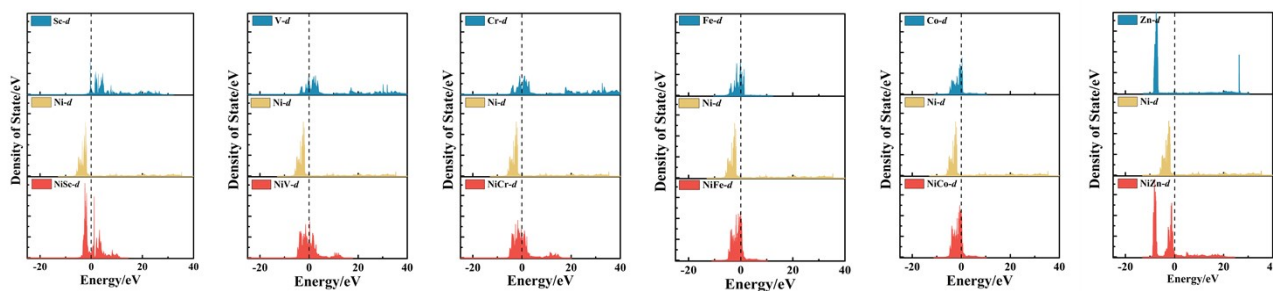


Figure S3. The 3d band projected density of state of NiSc(V, Cr, Fe, Co, Zn) bimetal bulk. The red: NiSc (V, Cr, Fe, Co, Zn)-3d band; the yellow: pure Ni-3d band; the blue: pure Sc(V, Cr, Fe, Co, Zn)-3d band. The bash line is Femi energy.

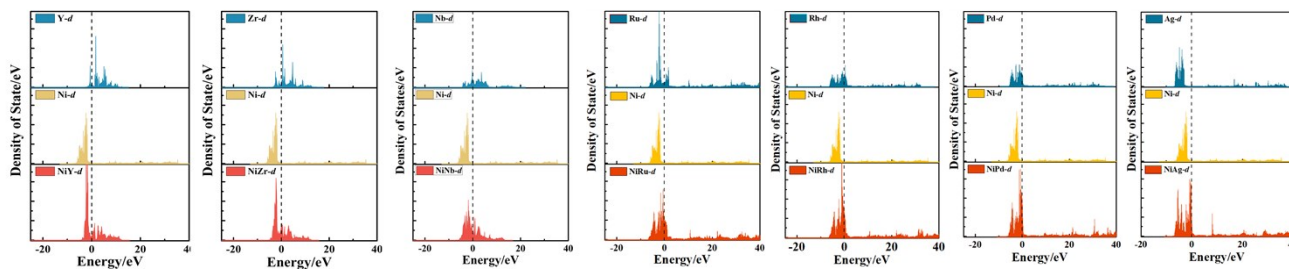


Figure S4. The 4d band projected density of state of NiY(Zr, Nb, Ru, Rh, Pd, Ag) bimetal bulk. The red: NiY(Zr, Nb, Ru, Rh, Pd, Ag)- 4d band; the yellow: pure Ni-3d band; the blue: pure NiY(Zr, Nb, Ru, Rh, Pd, Ag)- 4d band. The bash line is Femi energy.

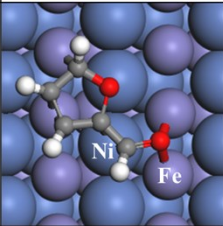
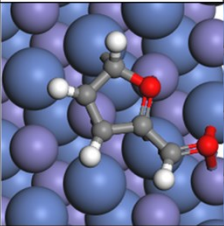
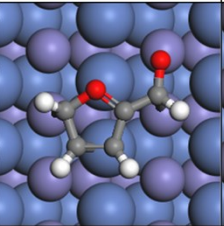
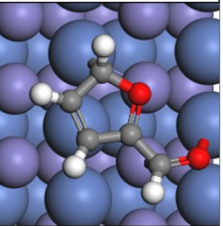
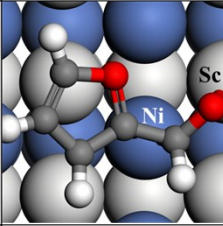
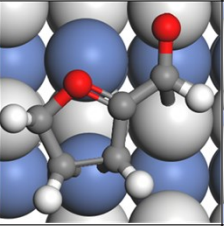
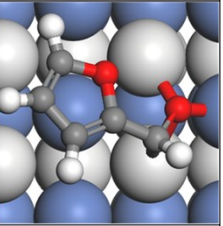
Site	Ni-Fe	Ni-Ni	Fe-Fe	Fe-Ni
Top view				
E_{ads}/eV	-1.91	-1.83	-1.86	-1.61
Site	Ni-Sc	Ni-Ni	Sc-Sc	Sc-Ni
Top view		/		
E_{ads}/eV	-2.89	/	-2.66	-2.46

Figure S5. Structures and adsorption energies of furfural absorbed on various adsorption sites based on NiFe(111) and NiSc(111) surface.

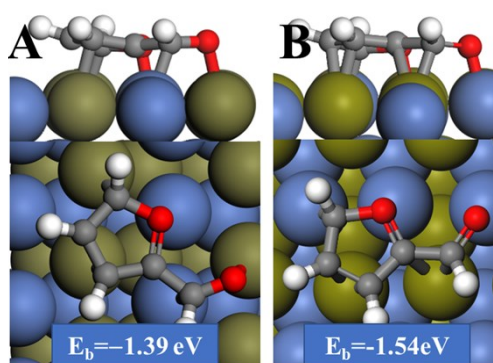


Figure S6. Structures and adsorption energies of furfural absorbed on Ni-Pd site and Pd-Ni site. A doped metal is noble metal, the most stable adsorption structure is the bind of C-Pd and O-Ni(B).

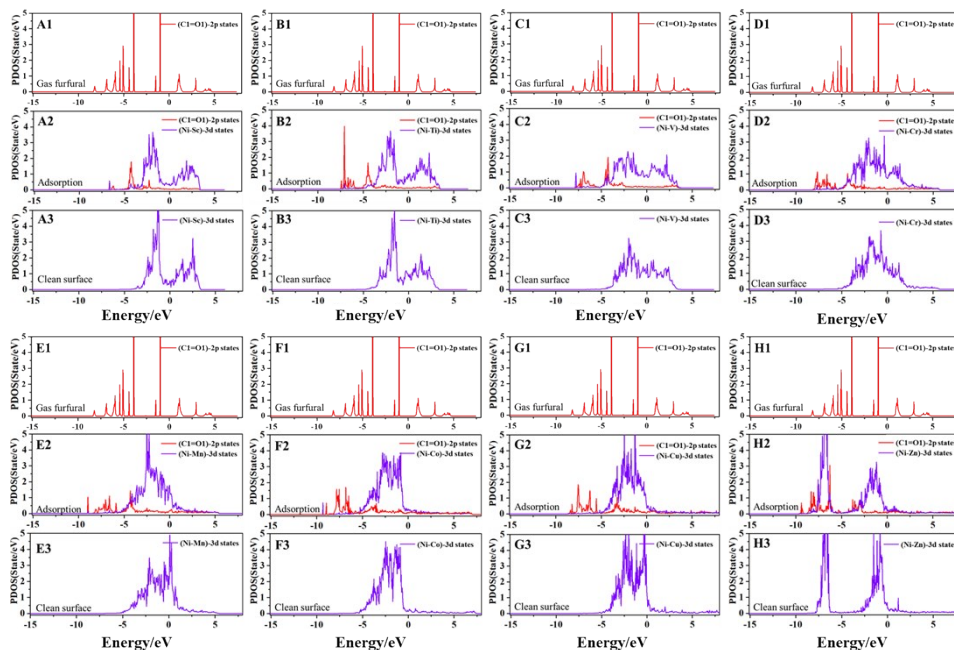


Figure S7. Projected density of states (PDOS) for C1=O1 in gas FAL (A1), in adsorbed FAL on Ni-M (A2-Sc, B2-Ti, C2-V, D2-Cr, E2-Mn, F2-Co, G2-Cu and H2-Zn), and the PDOS of Ni-M in clean surface (A3-H3).

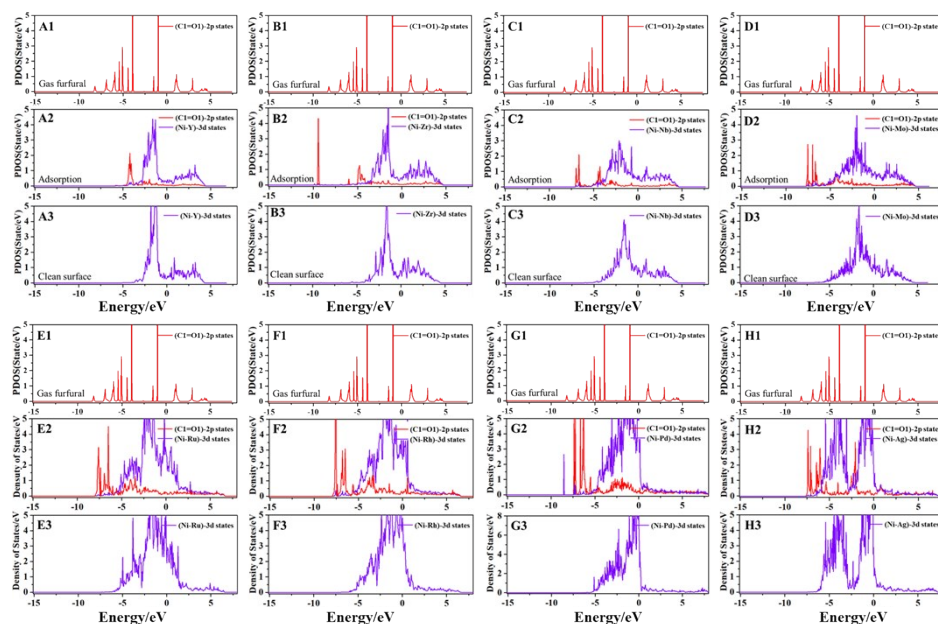


Figure S8. Projected density of states (PDOS) for C1=O1 in gas FAL (A1), in adsorbed FAL on Ni-M (A2-Y, B2-Zr, C2-Nb, D2-Mo, E2-Ru, F2-Rh, G2-Pd, and H2-Ag), and the PDOS of Ni-M in clean surface (A3-H3).

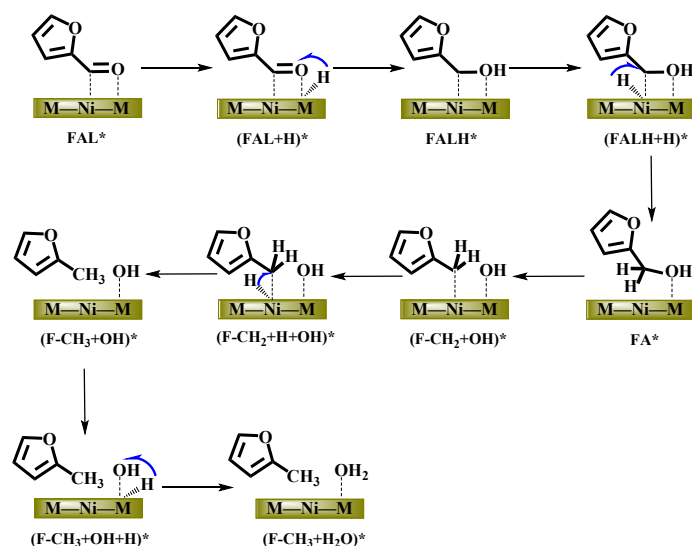


Figure S9. The elementary steps and reaction process for FAL conversion to 2-MF involves three main chemical process, hydrogenation, C-OH scission, and finally hydrogenation to product.

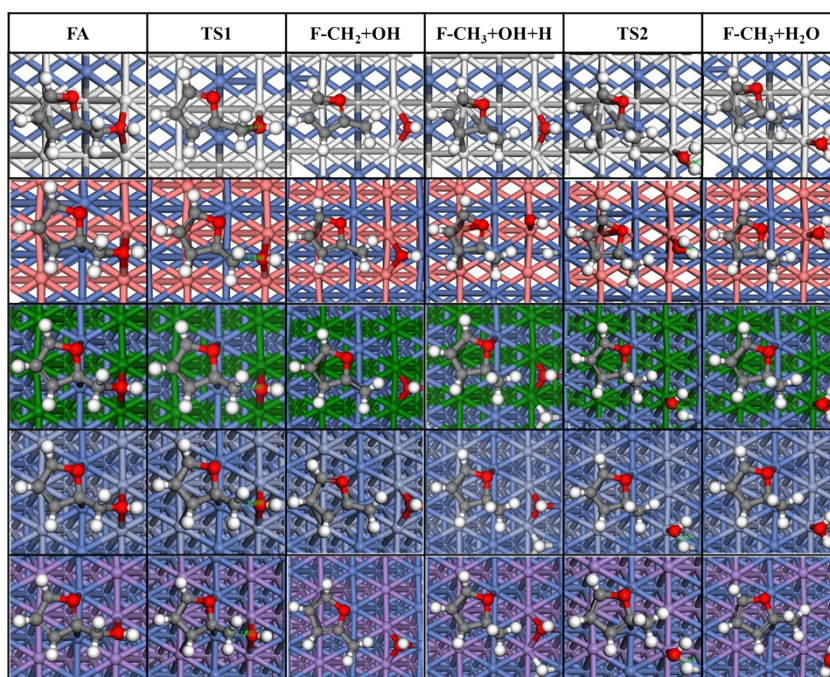


Figure S10. The structures of reactants, TS, and products for the conversion of FAL to 2-MF on Ni-M (M = Sr, Ti, V, Cr, Mn).

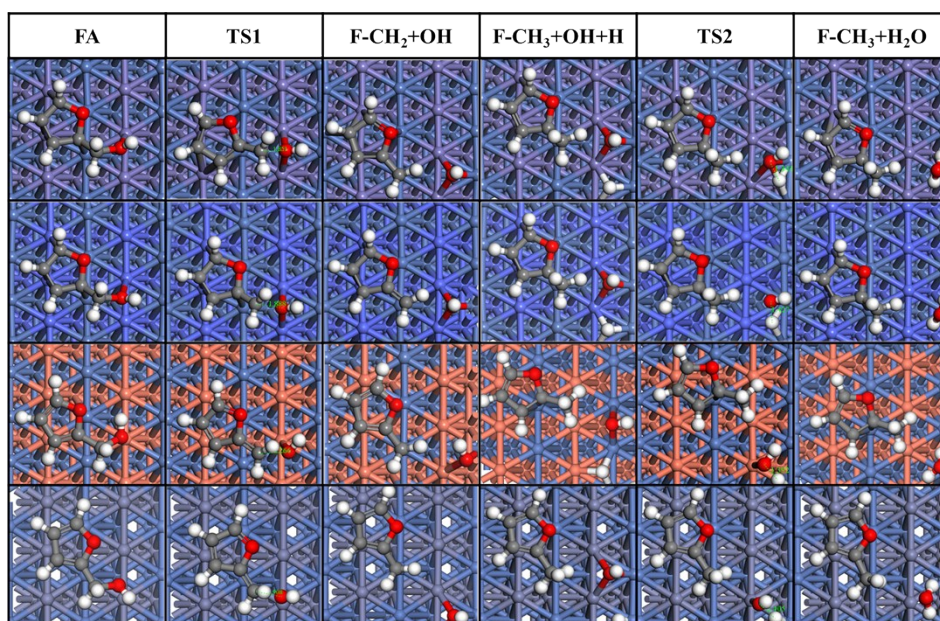


Figure S11. The structures of reactants, TS, and products for the conversion of FAL to 2-MF on Ni-M (M = Fe, Co, Cu, Zn).

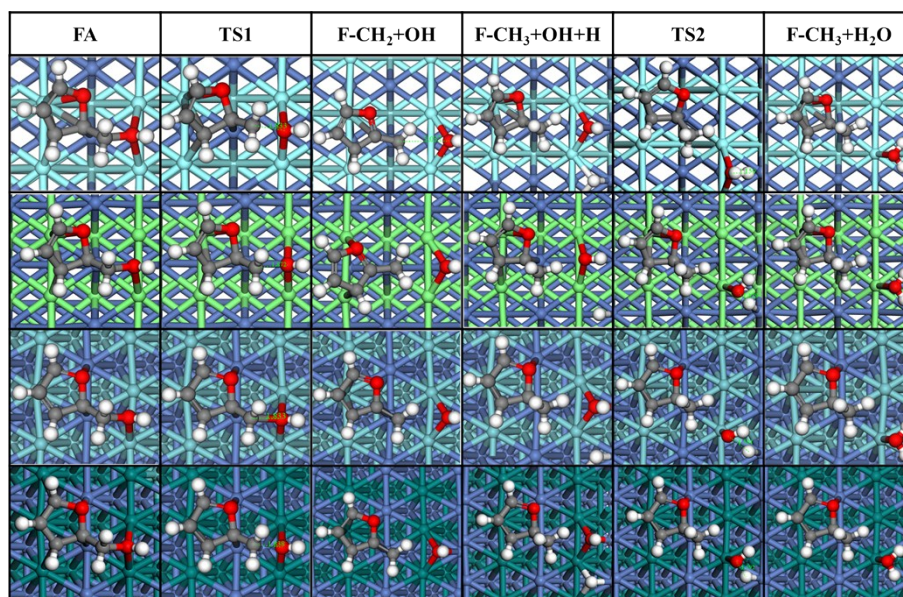


Figure S12. The structures of reactants, TS, and products for the conversion of FAL to 2-MF on Ni-M (M = Y, Zr, Nb, Mo).

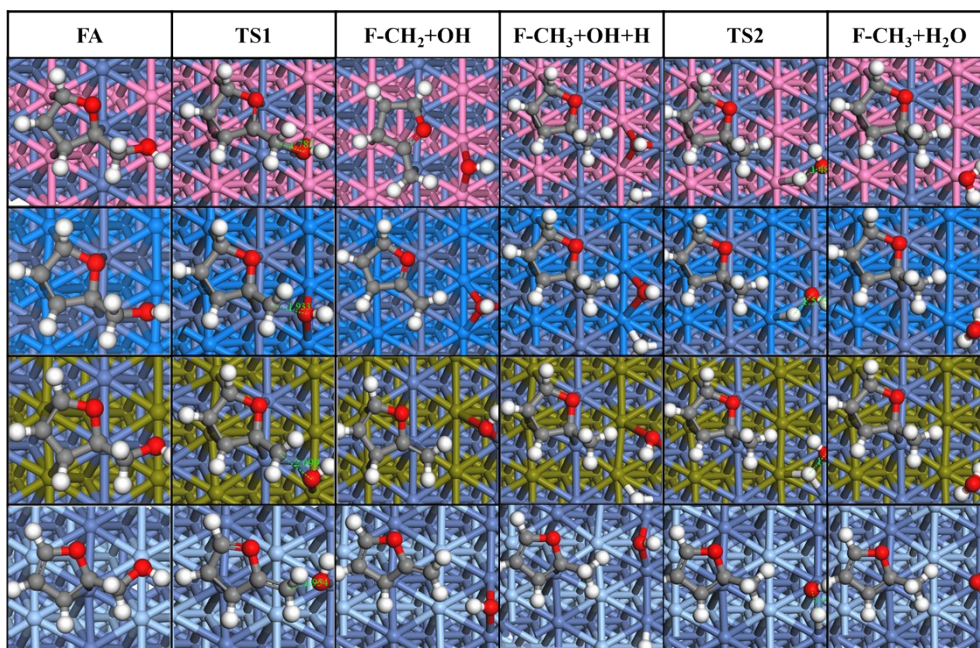


Figure S13. The structures of reactants, TS, and products for the conversion of FAL to 2-MF on Ni-M (M = Ru, Rh, Pd, Ag).

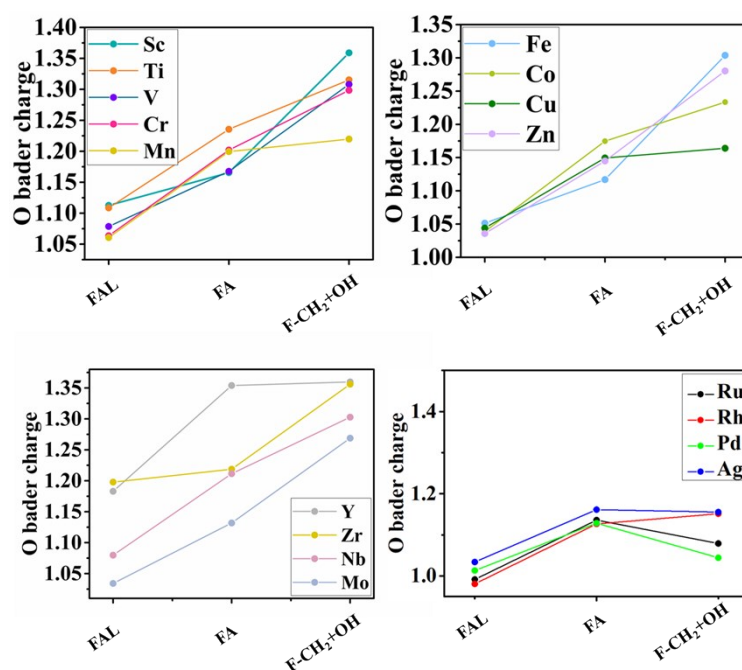


Figure S14. The change of O Bader charge in whole reaction process.

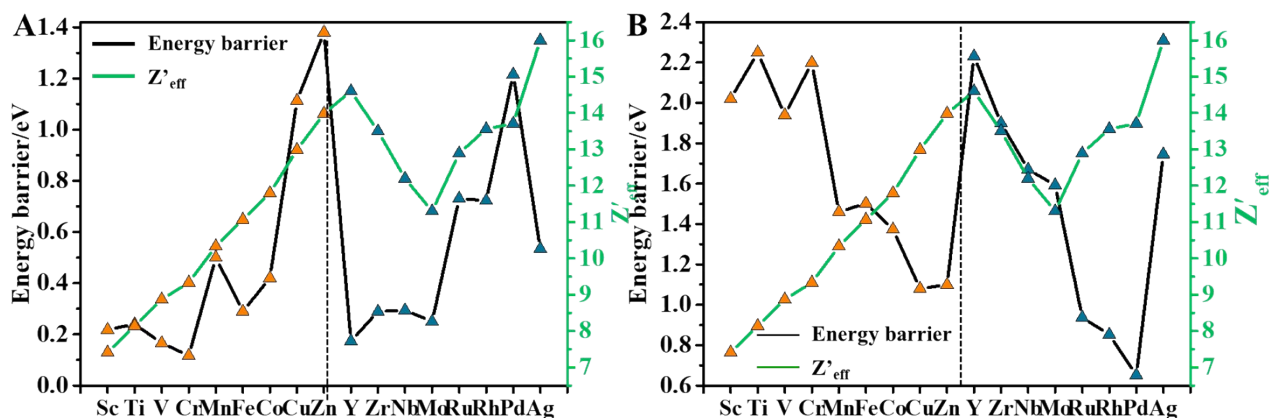


Figure S15. Relationship between element order and energy barrier (left side)/the effective nuclear charge (Z'_{eff}) (right side), Z'_{eff} from the compilation by Clementi et al^{3,4}. (A) for C-OH scission, (B) for *OH species hydrogenation. Orange represents Ni-M (M=3d elements); blue represents Ni-M (M=4d elements).

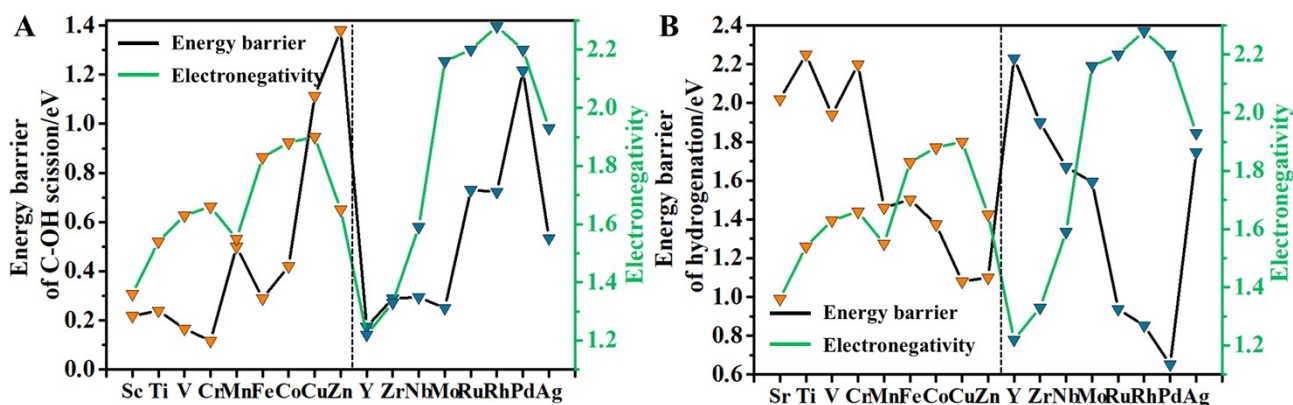


Figure S16. Relationship between element order and energy barrier (left side)/electronegativity (right side). (A) for C-OH scission, (B) for *OH species hydrogenation. Orange represents Ni-M (M=3d elements); blue represents Ni-M (M=4d elements).

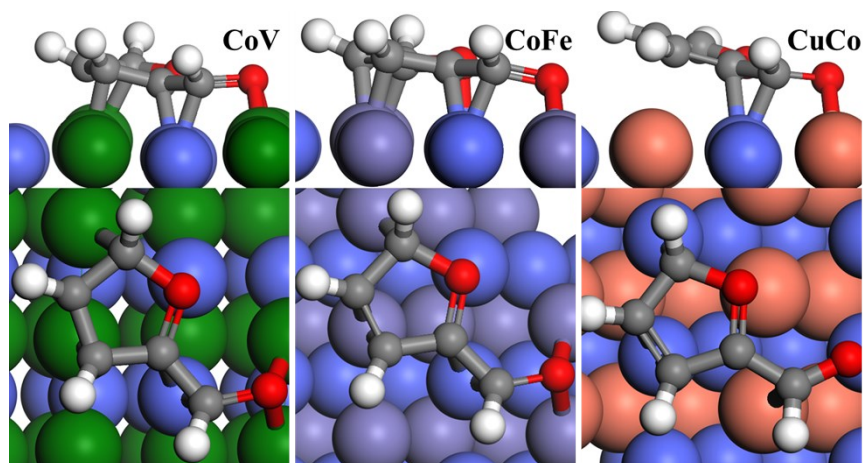


Figure S17. Adsorption structures of FAL on the surface of CoV, CoFe, and CuCo bimetallic catalysts.

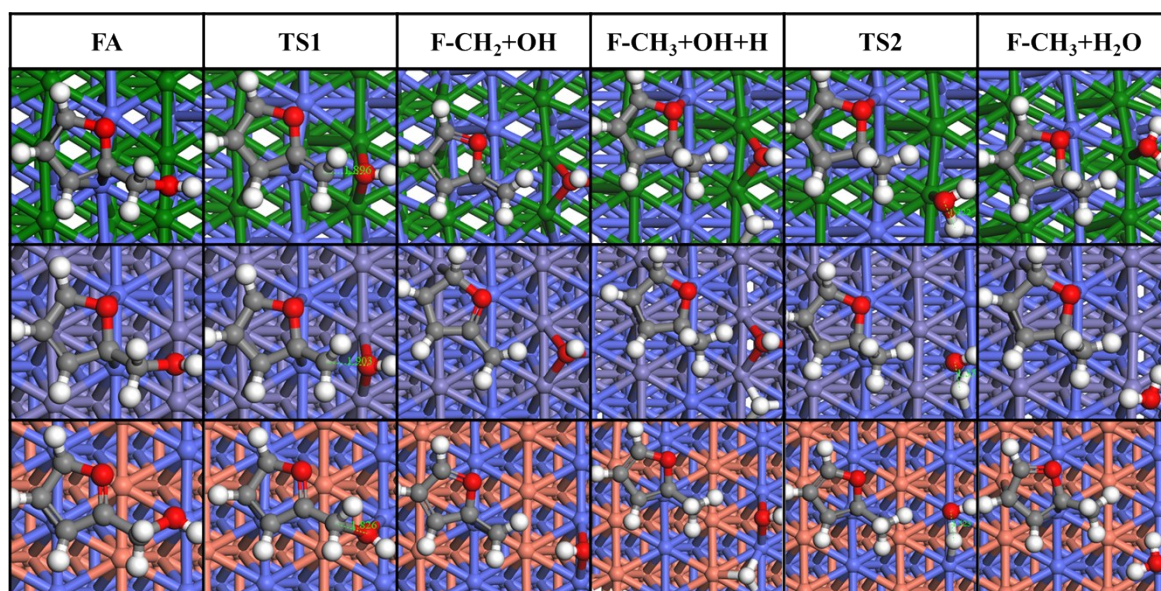


Figure S18. The structures of reactants, TS, and products for the conversion of FAL to 2-MF on CoV, CoFe, and CoCu bimetallic catalysts.

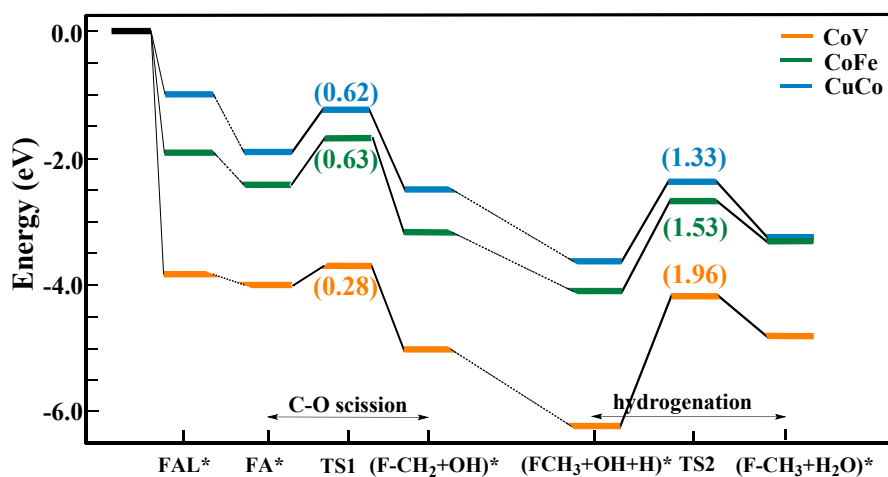


Figure S19. Potential energy profiles (in eV) for FAL conversion to 2-MF on CoV(111), CoFe(111), and CuCo(111) surfaces.

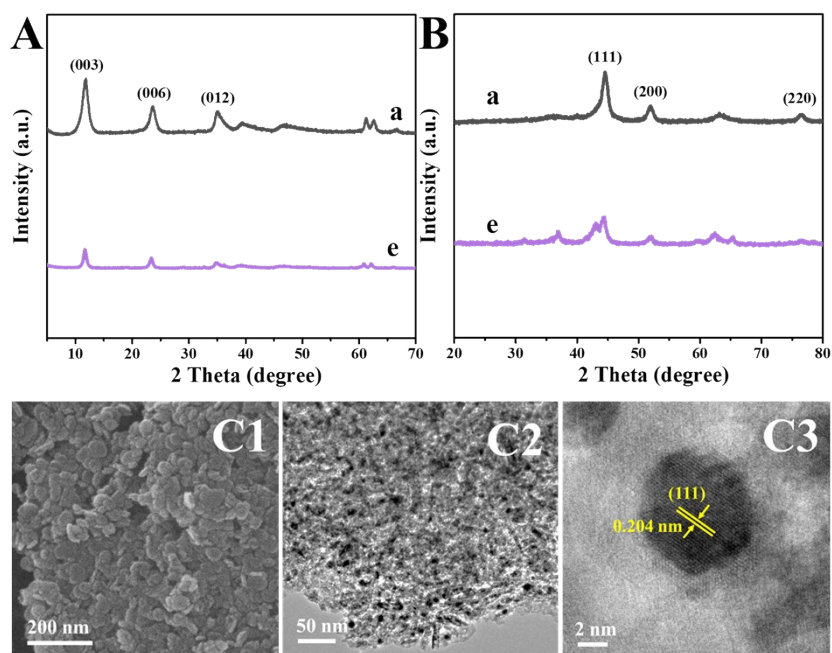


Figure S20. (A). XRD patterns of the as-synthesized LDHs precursors: (a) $\text{Ni}_{0.5}\text{Mg}_{1.5}\text{Al}_1$ -LDHs, (e) $\text{Ni}_{0.5}\text{Mn}_{0.5}\text{Mg}_{1.5}\text{Al}_{0.5}$ -LDHs. (B) XRD patterns of the resulting Ni and Ni-based alloys: (a) Ni/MgAl-MMO, (e) NiMn/MgAl-MMO. SEM, TEM and HRTEM images of the resulting Ni and Ni-based alloys: (C1-C3) NiMn/MgAl-MMO.

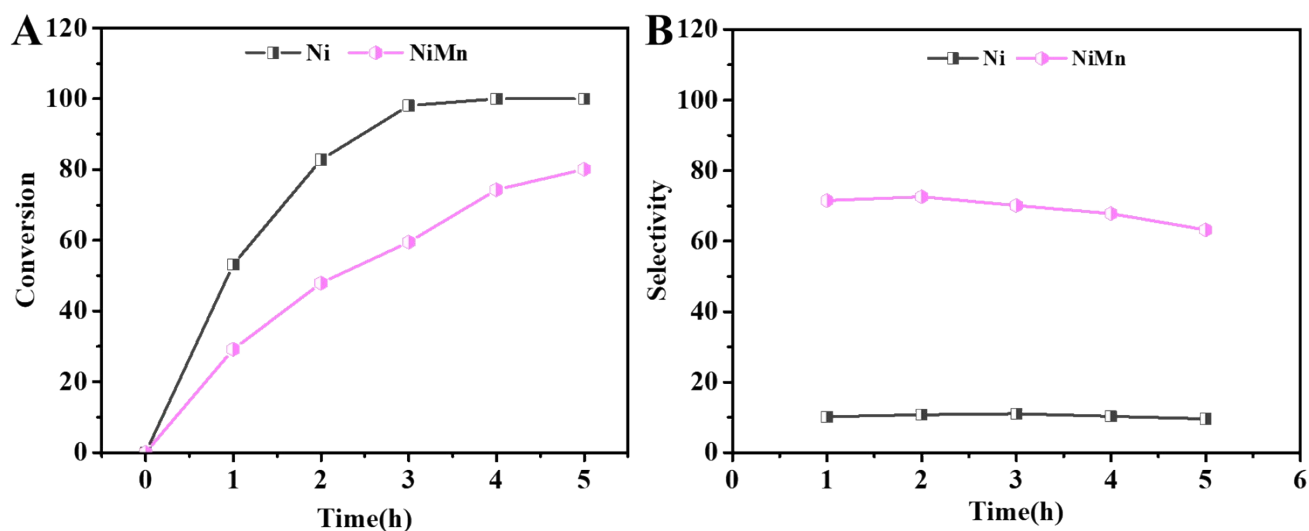


Figure S21. (A) Catalytic conversion and (B) corresponding selectivity vs. reaction time for FA hydrogenation over monometallic Ni and NiMn alloys.

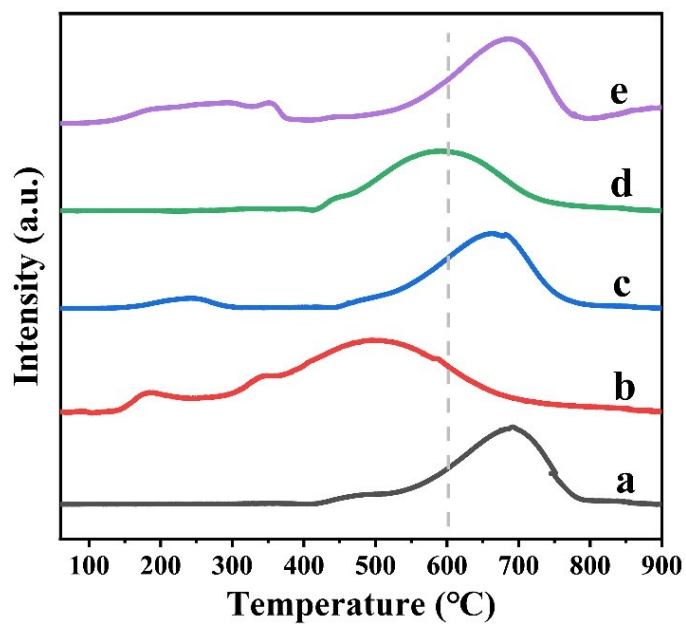


Figure S22. H₂-TPR profiles of (a) Ni, (b) NiCu, (c) NiCo, (d) NiZr and (e) NiMn., respectively.

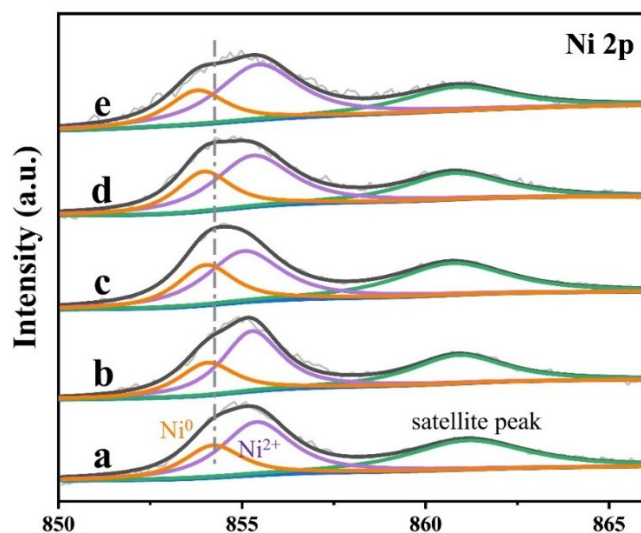


Figure S23. (A) Ni 2p X-ray photoelectron spectroscopy (XPS) of various samples: (a) Ni, (b) NiCu, (c) NiCo, (d) NiZr and (e) NiMn.

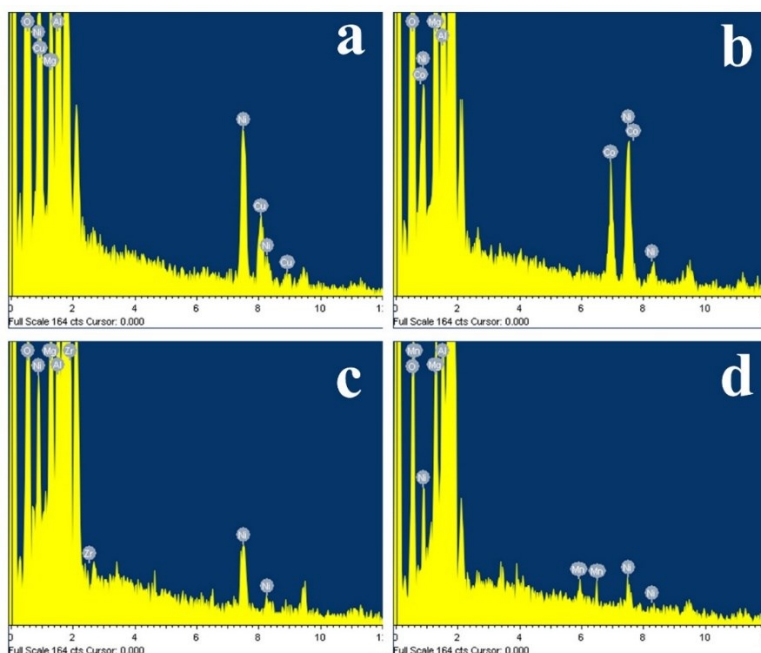


Figure S24. Energy Dispersive Spectroscopy (EDS) of various samples: (a) NiCu, (b) NiCo, (c) NiZr and (d) NiMn.

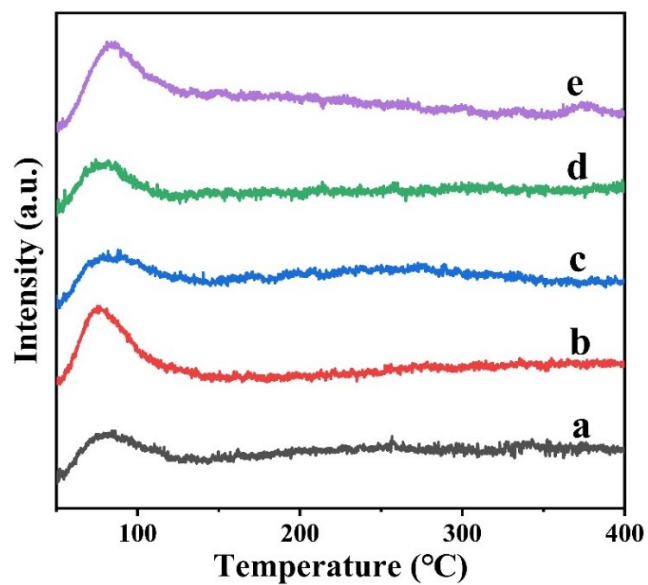


Figure S25. H₂-TPD profiles of (a) Ni, (b) NiCu, (c) NiCo, (d) NiZr and (e) NiMn., respectively.

REFERENCES

- [1] I. K. Suh, H. Ohta, Y. Waseda, *J. Mater. Sci.* 1988, **23**, 757.
- [2] S. D. Miller, J. R. Kitchin, *Surf. Sci.* 2009, **603**, 794.
- [3] E. Clementi, D. L. Raimondi, *J. Chem. Phys.* 1963, **38**, 2686–2689.
- [4] E. Clementi, D. L. Raimondi, W. P. Reinhardt, *J. Chem. Phys.* 1967, **47**, 1300–1307.